WARWICK
THE UNIVERSITY OF WARWICK

Maximum power point tracking (MPPT) control of pressure retarded osmosis (PRO) salinity power plant: development and comparison of different techniques

Wei He [a, b,*], Xing Luo [a], Oleh Kiselychnyk [a], Jihong Wang [a], Mohammad Hasan Shaheed [b,*]

[a] *School of Engineering, University of Warwick, Coventry, CV4 7AL, UK*

[b] *School of Engineering and Material Science, Queen Mary University of London, London, E1 4NS, UK*

Abstract:

This paper presents two new methods for the maximum power point tracking (MPPT) control of a pressure retarded osmosis (PRO) salinity power plant, including mass feedback control (MFC) and fuzzy logic control (FLC). First, a brief overview of perturb & observe (P&O) and incremental mass resistance (IMR) control is given as those two methods have already demonstrated their merit in good control performance. Then, two new methods employing variable-step strategy, MFC and FLC, are proposed to address the trade-off relationship between rise-time and oscillation of P&O and IMR. Genetic Algorithm (GA) is used for finding the optimum parameters of membership functions of FLC. From the case-study of start-up of the PRO adopting MPPT control, MFC and FLC have shown faster convergence to the target performance without oscillation compared with P&O and IMR. These four MPPT techniques are further evaluated in case-studies of state transitions of the PRO due to operational fluctuations. It is proven that the MPPT using FLC and modified MFC has better performance than the other two methods. Finally, the paper reports a comparison of major characteristics of the four MPPT methods, which could be considered as guidance for selecting a MPPT technique for the PRO in practice.

Keywords: Pressure retarded osmosis, Maximum power point tracking, Mass feedback control, Fuzzy logic control, Genetic algorithm

---

[*] Corresponding author: Tel: + 44(0)20 7882 3774(W He), +44 (0)20 7882 3319(MH Shaheed)
 E-mail address: w.he.1@warwick.ac.uk m.h.shaheed@qmul.ac.uk

1. Introduction

Pressure retarded osmosis (PRO) is a promising method which is potentially capable of producing power and processing water simultaneously because of its nature of combination of the water treatment and renewable energy generation. In other words, it can be used as not only a clean energy generator, but also a water treatment to recycle water. In a PRO plant, chemical potential between the two salinities is converted to hydraulic potential which is harvested using hydro-turbines. The energy conversion and the water recycle are based on the transportation of the pure water from the low concentration side to the high concentration side, due to the higher osmotic pressure difference across the membrane than the hydraulic pressure applied on the draw solution.

Generation of salinity power, or osmotic power, using PRO has been widely investigated in the last five years. It is reported that the economic viability can be achieved if the power density is higher than 5 W/m^2 [1]. The commercial reverse osmosis (RO) membranes and forward osmosis (FO) membranes are inappropriate for the PRO applications because of different operational conditions. The bulky support layers of the RO membranes cause severe internal concentration polarization (ICP) and significant decrease in water flux. In contrast, the highly open substrate of the FO membranes does not possess the sufficient mechanical strength to withstand the pressure applied in the PRO process. Therefore, in order to realise the PRO process in practice, first, specific high performance membranes for the PRO process have been investigated. Recently, Li et al. developed a TFC polyetherimide PRO flat–sheet membrane which is able to maintain almost unchanged water flux and power density of 12.8 W/m^2 at 17.2 bar over 10 hours [2]. While maintaining a relatively small structural parameter to minimize ICP, enhancing membrane water permeability during the formation of polyamide layers and/or novel post-treatment is also important [3]. Cui et al. optimized the interfacial polymerization reaction and alternative post-treatments, and fabricated a membrane with power density of 18.09 W/m^2 at 22 bar when using 1 M NaCl as draw solution and DI water as feed [4]. A comprehensive review of the development of the high performance PRO membranes can be found in [3].

The process characteristics of the PRO and the optimization of the configuration and operation are the second step to develop practical applications taking advantages of the fabricated high performance membranes. Compared to the lab-scale PRO process, mass transfer of the water and salts across the membrane is highly affected by the increasing membrane usage and the hydrodynamic flows of the salinities. It is reported that although the total extractable energy capacity of the PRO is enhanced with the increase of the membrane area, the average membrane power density is significantly decreased due to the rapidly vanishing net driving force [5]. Sivertsen et al. constructed an iso-watt diagram of PRO as a map to link the membrane properties and the lab-scale membrane performance [6]. Furthermore, He et al. constructed an operation map of the scale-up PRO process to identify the coupled effects of the increased process scale with the membrane properties [7]. These operation maps nicely illustrated the characteristics of the PRO from lab-scale to the scale of practical applications. Moreover, to mitigate the detrimental effects of ICP, external concentration polarization (ECP) and reverse solute permeation (RSP), different configurations have been studied to enhance the overall performance of the system. Hybrid RO-PRO is one of the widely investigated configuration due to the inherently benefiting performance of the two processes [8]. Achilli et al. carried out both numerical and experimental investigations on the hybrid RO-PRO plant [9, 10]. The maximum power density of PRO can be approximately achieved up to 10 W/m^2 in the simulations of hybrid system by using virtual membrane [9]. While in the pilot system, average experimental power densities for the RO-PRO process ranged from 1.1 to 2.3 W/m^2 [10]. Altaee et al.

carried out systematic modelling and optimization of dual-stage PRO process [11-14] and hybrid FO/RO/PRO process [15, 16]. PRO also shows promising performance in other hybrid processes. In a novel PRO-MD (membrane distillation) hybrid process, the maximum power densities of 31.0 W/m^2 and 9.3 W/m^2 by the PRO using DI water and real wastewater mixing with 2M NaCl concentrate [17]. In another hybrid multi-stage vacuum MD and PRO process, maximum power density of 9.7 W/m^2 is achieved when river water is used as feed solution [18]. Recently, a preliminary investigation of hybrid photovoltaic (PV) solar and PRO osmotic energy has been proposed and studied. The demonstrated benefiting improvements of both renewable energy generation and water desalination especially push the osmotic power to the market [19].

Accordingly, based on the significantly improved membrane performance and the increasingly clear understanding of the process characteristics of the scale-up PRO, another key step to push the technology realisation in practical applications is control of input variables of the PRO, such as hydraulic pressure applied on the draw solution, to ensure the optimized performance. In fact, studies focusing on optimal control have been important topics of research in solar, wind, wave, tidal, and other renewable energy generations. But due to the difficulty of deriving the analytical solutions for complex systems, the stable, robust and efficient maximum power point tracking (MPPT) systems represent a challenge for renewable energy designers. MPPT is used to operate the renewable energy generators in a manner to maximize the output power, irrespective of the operational fluctuations and variations. According to the significant development in last decades, several algorithms have been developed in tracking the maximum power point (MPP) for not only solar PV arrays [20-26] but also for fuel cell power plant [27, 28]. In this context, in order to maximize the performance of PRO in practice, MPPT controller is essential to ensure the design operation and performance of a PRO power plant. However, at the early stage of studying the MPPT in PRO, there is very limited work reported in the literatures. In our previous study, two algorithms for MPPT in a PRO are proposed and investigated, including perturb & observe (P&O) algorithm and incremental mass resistance (IMR) algorithm [29]. It is demonstrated by simulations that both P&O and IMR algorithms can be used to track the MPP of a PRO process at the steady-state operations and the transiting operations due to the operational fluctuations. But the trade-off between the rise time and the oscillation by selecting the step-size of the perturbation pressure or incremental pressure exists in both algorithms. Larger step-size results in fast response as well as larger oscillation, and vice versa.

Therefore, in this study, in order to balance the trade-off relationship between the rise-time and oscillation, two new MPPT controllers, mass feedback control (MFC) and fuzzy logic control (FLC), are developed and compared with P&O and IMR methods. First, the four methods are introduced, in which algorithms of MFC and FLC are described in details. For the MPPT using FLC, genetic algorithm (GA) is used to search for the optimum parameters for the settings of the membership functions. Then, two case studies are carried out to evaluate the two new MPPT controllers and compare the four algorithms. Finally, as guidance for the designers and users to select a MPPT algorithm for a particular PRO application, a table that summaries the major characteristics of the methods is also provided.

2. Process characteristics of a PRO salinity power plant

Fig. 1 shows the characteristic power curve for a scale-up PRO plant. The problem considered by MPPT techniques is to automatically find the applied pressure (P_{MPP}) at which a PRO power plant should operate to achieve the MPP ($\overline{W}_{MPP}$) under the given operational condition. Furthermore, due

to the fluctuations of the operations, such as temperature, pressure and flow conditions, the MPP also varies. Therefore, the MPPT controller is required not only to fast reach the MPP at the start-up process but also automatically respond to changes in the process due to operation fluctuations. Moreover, once the MPP is found, a smooth operation with insignificant oscillation needs to be maintained by the MPPT controller.
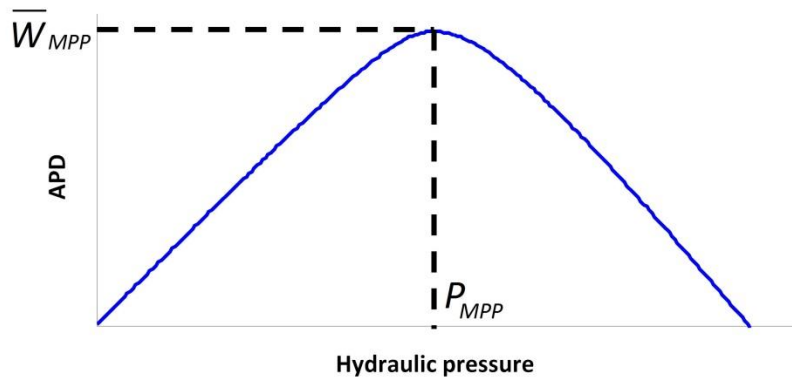

Figure 1 Characteristic PRO power curve.

3. MPPT control

The four MPPT control algorithms considered in this study are introduced in this section, including two previously developed methods in [29], P&O and IMR, and two new methods, MFC and FLC. P&O and IMR are briefly introduced below and details of the two algorithms can be found in [29].

3.1. Perturb & observe

P&O involves a perturbation in the applied pressure on the draw solution to search for the MPP of the PRO salinity power generator. Incrementing (decrementing) the applied pressure increases (decreases) the power when operating on the left of the MPP and decreases (increases) the power when on the right of the MPP. Therefore, if the measured power is increasing at the sample instant, the subsequent perturbation should be kept the same to reach the MPP and if the measured power is decreasing, the perturbation should be reversed. The P&O based MPPT method is summarised in Table 1. The P&O process is repeated based on the algorithm until the MPP is reached. Due to the perturbation size, an oscillation is always accompanied. A larger perturbation pressure leads to fast convergence but a larger oscillation as well. In contrast, a smaller perturbation pressure slows down the MPPT.

Table 1 Direction of pressure perturbation of P&O.

Change in power / Perturbation Pressure	Positive	Negative
Positive	Positive	Negative
Negative	Negative	Positive

3.2. Incremental mass resistance

IMR is based on the fact that the slope of the PRO power curve is zero at the MPP, positive on the left of the MPP, and negative on the right, as given by

$$d\overline{W}/dP = 0, \qquad \text{at MPP}$$
$$d\overline{W}/dP > 0, \qquad \text{left of MPP} \qquad (1)$$
$$d\overline{W}/dP < 0, \qquad \text{right of MPP}$$

Because of the slope of the PRO power curve can be also approximated by the incremental pressure, pressure, flow rate and the flow rate change, which is presented as,

$$\frac{d\overline{W}}{dP} = \frac{d(PV)}{A_M dP} = \frac{1}{A_M}(V + P\frac{dV}{dP}) \cong \frac{1}{A_M}(V + P\frac{\Delta V}{\Delta P}) \qquad (2)$$

where V presents the volumetric flow rate. With a fixed membrane area, equation (1) can be rewritten as

$$\Delta P/\Delta V = -P/V \quad \text{or} \quad \Delta V/\Delta P = -V/P, \qquad \text{at MPP}$$
$$\Delta P/\Delta V < -P/V \quad \text{or} \quad \Delta V/\Delta P > -V/P, \qquad \text{left of MPP} \qquad (3)$$
$$\Delta P/\Delta V > -P/V \quad \text{or} \quad \Delta V/\Delta P < -V/P, \qquad \text{right of MPP}$$

where P/V and $\Delta P/\Delta V$ are defined as the instantaneous mass resistance and the incremental mass resistance, respectively. Mass resistance refers to the difficulty to pass a particular flow rate of the permeation through the membrane in a PRO. The inverse quantity of the resistance is mass conductance, describing the ease with which a current of the permeation passes. Therefore, the MPP can be tracked by either comparing the instantaneous mass resistance (P/V) to the incremental mass resistance ($\Delta P/\Delta V$) or comparing the instantaneous mass conductance (V/P) to the incremental mass conductance ($\Delta V/\Delta P$), as shown in equation (3). In fact, the two comparisons are equivalent in mathematics and mass resistance, namely IMR, is selected in this study to calculate the slope of the PRO power curve. A flowchart of the algorithm is shown in Fig. 2. On one hand, similar to the P&O algorithm, the incremental pressure determines the convergence of the MPPT. Fast tracking can be achieved with larger increments but accompanying with an oscillation. Therefore, how to select the incremental pressure is a trade-off to balance the convergence and oscillation. On the other hand, control parameter in IMR, ε_{IMR}, can be used to decrease or eliminate the oscillation at certain levels without the sacrifice of the convergence. Therefore, compared to P&O algorithm, IMR is more flexible in MPPT. If a particular deviation of the MPP is acceptable, the stability of the MPPT can be significantly improved.
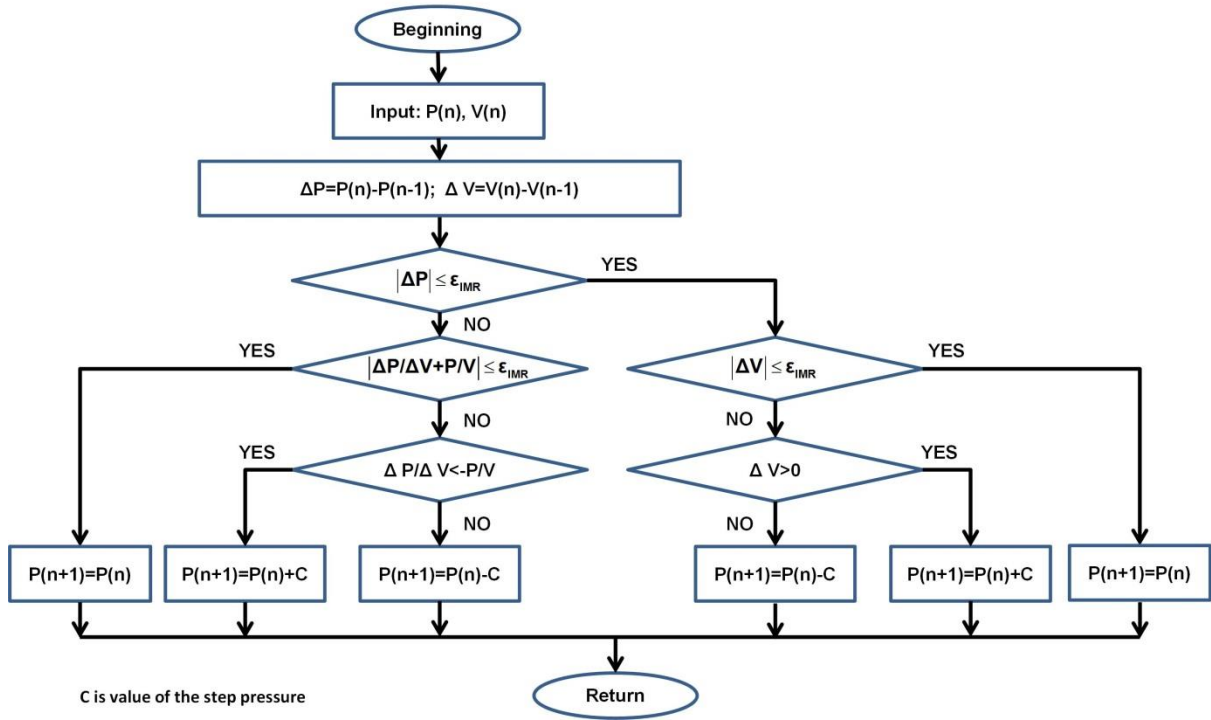
Figure 2 Flowchart of IMR algorithm. C is value of the step pressure.

3.3. Mass feedback controller

With DSP and microcontroller which are capable to handle complex computation, an obvious way of performing MPPT is to compute the slope of PRO power curve ($d\overline{W}/dP$) and feed it back to the step-pressure at the next sample instant to drive it to zero. The way to compute the slope and feedback is determined by the user. Inspired by the conventional PI control which attempts to minimize the error over time by adjustment of a control variable, a PI-like mass feedback control (MFC) is also proposed in this section. The aim of MFC is to minimize the slope of the PRO power curve over time by adjusting the step-pressure. Therefore, the algorithm below is used for MFC,

$$\Delta P(n) = k_p [(\frac{d\overline{W}}{dP})_n - (\frac{d\overline{W}}{dP})_{n-1}] + k_i (\frac{d\overline{W}}{dP})_n \tag{4}$$

where k_p, and k_i both non-negative, denote the coefficients for the proportional and integral gains, respectively. Unlike IMR algorithm that use only the sign of the slope, MFC effectuates an adaptive gain that the fast convergence achieves, the further the position of the actual operation point is from the MPP. In the proposed MFC, the step-pressure is the sum of two terms: the first term is proportional to the change of the slope and the second term is proportional to the slope.

3.4. Fuzzy logic control

A new MPPT controller for a PRO salinity power plant based on fuzzy logic is proposed in this section. Fuzzy logic control (FLC) is a non-model based control method, which attempts to employ the expert knowledge of the experienced operators to derive the control rules. FLC has the advantages of allowable imprecise inputs, free of accurate mathematical models, and handling non-

linearity. Generally, as depicted in Fig. 3, a FLC normally consists of four main steps/components: 1) Fuzzification. A fuzzifier is designed to map crisp values of the inputs into fuzzy sets to activate rules; 2) FLC rules. The rules are defined to design the FLC behaviour by using a set of IF-THEN statements of the FLC rules; 3) Inference. Based on the rules, the inference engine maps the input fuzzy sets into output fuzzy sets; 4) Defuzzification. A defuzzifier is applied to map output fuzzy sets into crisp values.
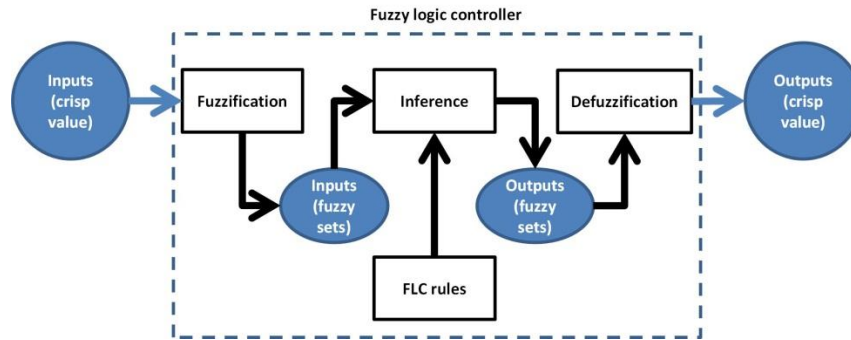

Figure 3 Block diagram of the fuzzy logic control

The rules are the key components to determine the FLC operation, which is expressed as linguistic variables in terms of fuzzy sets. The output is obtained by applying an inference mechanism, which includes [30]: membership functions, connections linking the rules antecedents, implication function and rule aggregation operator. The membership functions are usually piece-wise linear function associated to the FLC linguistic variables, such as triangular or trapezoidal functions. The number and the shape of the membership functions of each fuzzy set as well as fuzzy logic inference mechanism are selected by the operators and thus the performance of the FLC depends on the experiences of the designers. The searching rules formulation in this work is based on the PRO power curve as shown in Fig. 1. If the last change in the applied pressure causes the power to rise, keep searching in the same direction; otherwise, if the last change causes the power to drop, move to the opposite direction.

The FLC control is achieved based on satisfaction of two criteria relating two input variables, namely slope and change of slope, at a particular sampling instant. Similar to the error and the change of the error in the conventional FLC, the controller drives these two variables to zeros when the steady-state MPP is reached. Therefore, at the sampling instant n, the two variables, slope (E) and change of slope (ΔE) are expressed as

$$E(n) = \frac{\overline{W}(n) - \overline{W}(n-1)}{P(n) - P(n-1)} \tag{5}$$

$$\Delta E(n) = E(n) - E(n-1) \tag{6}$$

The slope in the FLC is expressed by an approximation of the slope of the PRO power curve, as shown in equation (5). And the change of the slope can obtained by equation (6) accordingly. Through the process of fuzzification, these input variables are expressed in terms of linguistic variables which are PB (positive big), PS (positive small), ZE (zero error), NS (negative small), and NB (negative big) using basic fuzzy subset. Fig. 4 illustrates the membership functions associated to the five linguistic variables for two inputs and one output. In the defined membership functions,

trapezoidal-shaped membership function is selected for fuzzy sets of NB and PB, and triangular-shaped membership function is selected for fuzzy sets of NS, ZE and PS. The parameters of these membership functions are based on the range of values of the numerical variables.
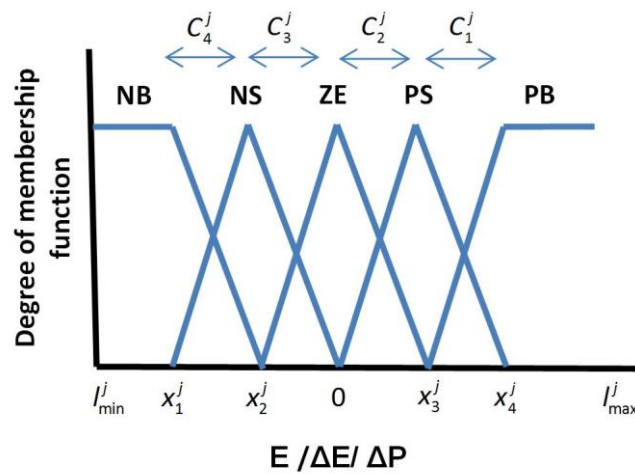

Figure 4 Illustrated membership functions of the input variables, E and ΔE, and the output variable, ΔP.

The pre-defined rules are important to determine the output step-pressure subject to different operations. The look up table of the rules used in this study is shown in Table 2, in which the linguistic variables assigned to step-pressure for the different combinations of the slope and the change of the slope are based on the knowledge and experiences of the users. As shown in the table, for example, the operating point is far to the left of the MPP, that the slope is PB, and the change of the slope is ZE, then a relatively large positive perturbation pressure should be added that is perturbation pressure should be PB to reach the MPP.

Table 2 Fuzzy rule based look up table.

Change of slope / Slope	NB	NS	ZE	PS	PB
NB	ZE	ZE	NB	NB	NB
NS	ZE	ZE	NS	NS	NS
ZE	NS	ZE	ZE	ZE	PS
PS	PS	PS	PS	ZE	ZE
PB	PB	PB	PB	ZE	ZE

For a FLC based MPPT, despite the operator expertise and knowledge at the level of rule-based inference and the membership functions, the settings of parameters are still very tedious. To improve the performance, one method is trial and error, which needs a large number of tests and simulations. The time to get optimum parameters depends on the experiences of the designers. Another method is to use the optimization method which generates and evaluates a series of tests automatically and search for the optimum parameters. In this study, genetic algorithm (GA) is used to find the optimum parameters [31]. The criterion of the optimization is to minimize the error at a selected operation condition,

$$f = \int e^2 dt = \int (\overline{W}_{MPP} - \overline{W})^2 dt \approx \sum_{n=1}^{N} (\overline{W}_{MPP} - \overline{W}(n))^2 \tag{7}$$

where $\overline{W}$ is the average power output, $\overline{W}_{MPP}$ is the MPP at the selected operation condition, and N is number of selected sample instants in optimization. In the future applications, the reference operation should be the design operation or the standard operation of a particular PRO power plant. In this study, the reference MPP is selected the steady-state MPP found by the MPPT using P&O. Number of sample instants to reach the MPP using P&O and IMR at the start-up process is varied with different perturbation pressure or incremental pressure [29]. The number of sample instants to reach the MPP using P&O is approximately between 5 to 20 in the start-up process using perturbation pressure of 5, 1, 0.5 bar from the initial pressure 1 bar [29]. Therefore, 20 sample instants are considered in the fitness function.

In order to improve the FLC performance, parameters of all the variables are optimized using GA. GA optimization employs the concepts of evolutionary theory, and provide an effective search in a large and complex solution space to obtain the optimum solutions. The algorithm is also known for avoiding local minima than gradient based algorithm. To use GA, parameters to be optimized need to be translated into chromosomes of an individual. Then a population of individuals which represent different possible parameters of variables to the minimization of the fitness function is evolved toward better design of FLC. Therefore, the population of GA optimization consists of a set of individuals, each of which has three chromosomes representing E, ΔE and ΔP. Because the same structure of membership functions are selected for inputs and output as shown in Fig. 4 in this study, chromosome uses the same presentation for all the three variables. Generally, the chromosome can be different to represent different designs of the membership functions of a variable to be optimized.

The five membership functions as shown in Fig. 4 can be expressed by six parameters including four parameters presenting the distances (C_k^{i1}, C_k^{i2} and C_k^o), the minimum (l_{min}^j) and the maximum (l_{max}^j). Therefore, an individual is composed of eighteen parameters which are illustrated in Fig. 5. The relation between C_k^{i1}, C_k^{i2} and C_k^o ($k=1,2,3,4$) and coordinates of the membership functions of the three variables, x_k^{i1}, x_k^{i2} and x_k^o are respectively given [30],

$$\begin{aligned}
x_1^j &= (C_4^j + C_3^j)l_{min}^j \\
x_2^j &= C_3^j l_{min}^j \\
x_3^j &= C_2^j l_{max}^j \\
x_4^j &= (C_1^j + C_2^j)l_{max}^j
\end{aligned} \tag{8}$$

where j presents the first input variables (i1) E, the second input variable (i2) ΔE and the output variable (o) ΔP. The parameters of C_k^{i1}, C_k^{i2} and C_k^o ($k=1,2,3,4$) are restricted and the minimums and maximums are determined by the users [30]. In this study, they are:

$$\begin{aligned}
&-0.3 \leq l_{min}^{i1}, l_{min}^{i2} < 0; \quad 0 < l_{max}^{i1}, l_{max}^{i2} \leq 0.3; \\
&-15 \leq l_{min}^o < 0; \quad 0 < l_{max}^o \leq 15; \\
&0 < C_k^{i1}, C_k^{i2}, C_k^o < 1, \quad k=1,2,3,4
\end{aligned} \tag{9}$$

$$\text{Individual}=[I_{min}^{i1},I_{max}^{i1},C_1^{i1},C_2^{i1},C_3^{i1},C_4^{i1},I_{min}^{i2},I_{max}^{i2},C_1^{i2},C_2^{i2},C_3^{i2},C_4^{i2},I_{min}^{o},I_{max}^{o},C_1^{o},C_2^{o},C_3^{o},C_4^{o}]$$

Figure 5 An illustrated individual used in GA optimization.

Therefore, based on equations (8), membership functions of the three variables can be represented by an individual in the population.

Moreover, with the defined individuals and fitness function, the optimization can be carried out. In GA, first an initial population is generated. A set of chromosomes should be randomly chosen to ensure the diversity of the solution candidates at the beginning. Then, GA uses the operations of selection, crossover and mutation to generate next generation. When the maximum value of the fitness functions is achieved with respect to a pre-defined value, the optimization is terminated. Otherwise, the optimization is working from generation to generation. In this study, the GA optimization is achieved using GA optimization toolbox of MATLAB. A population with 100 individuals has been taken to search for the optimum parameters. For the selection, the fitness function is set as equation (7). Selection function is stochastic uniform (*selectionstochunif*), in which each parent is chosen depending on a section of the line of length proportional to its scaled fitness value. Crossover fraction (*CrossoverFraction*) is used, which specifies the fraction of the next generation other than elite scheme. In order to make sure the coordinates x_1^j and x_4^j within the predefined range, a set of linear constraints are used for all variables, which are $C_1^j + C_2^j \le 1$ and $C_3^j + C_4^j \le 1$. And the upper and lower bounds for the parameters are set based on equation (9). According to the optimization toolbox, when the problem has linear/bound constraints, the mutation function *mutationadaptfeasible* is used. The settings of the toolbox are: Crossover fraction of each population 0.7, mutation fraction 0.3, and *TolFun* (tolerance of function), which is the average change of fitness function between two consecutive iterations and used as the stop criterion, 1×10^{-10}.

4. Evaluation and comparison of MPPT controllers

4.1. MPPT of a PRO salinity power generator

The aim of employing MPPT is to ensure that at any operational condition, maximum power is extracted from the PRO plant. Four algorithms aim to be evaluated and compared in this section. An illustrated diagram of a general MPPT controller used in the PRO is shown in Fig. 6. The MPPT evaluates the osmotic power generated by the hydro-turbine (HT) and adjust the applied hydraulic pressure on the draw solution. The pressure transition can be achieved by changing the displacement of the valves or/and using the variable frequency drive to change the speed of the high-pressure pump (HP) [32]. Based on the different algorithms of the MPPT controller, four different MPPT controllers introduced earlier, P&O, IMR, FLC and MFC, are used and studied to search the MPP. Two case studies are used to compare the performance of these MPPT controllers. This work aims to investigate the performance of the different MPPT algorithms by simulations. Therefore, at the early stage, all the algorithms of the MPPT are considered with the available measured pressures and flow rates. And the targeted pressure can be actuated on the draw solution

by a fast and stable controller. Current literatures suggested that the transition from one steady state to another steady state for RO process changes in different applications. Bartman et al. altered the flow rate less than ~1 min within a wide range of operation in UCLA experimental RO membrane water desalination system [33]. Sassi et al. reported that pseudo steady-state model of RO can be considered for time-step more than 0.25 h [34]. For PRO, currently there is no reported literature studying the transition between the operations. But due to the inherent similarity to RO desalination plant, the range of the transition time can be estimated. In this study, a general sample instant is used for representing the sensing period [29]. The sample instant is assumed to be larger than the transition time caused by applying the step pressure.
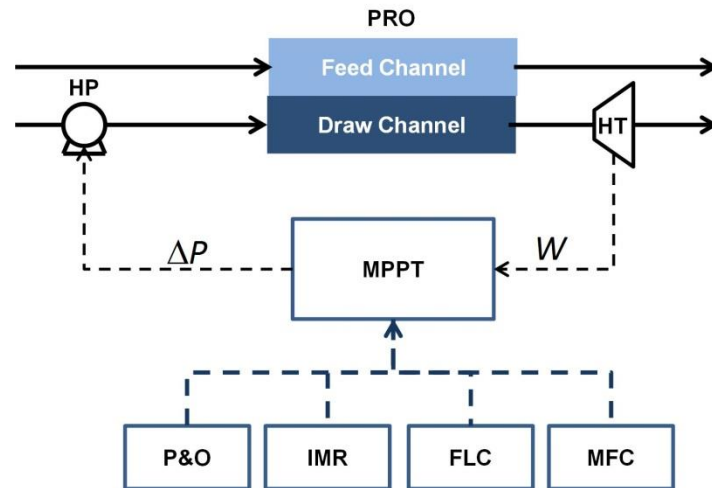

Figure 6 An illustrated PRO power plant using MPPT.

4.2. Case study of MPPT: start-up of a PRO salinity power generator

The parameters used in this section are shown in Table 3. The performance of the PRO salinity power generator is obtained based on the models and modelling framework developed in our previous work [35], which are described in Appendix A.1. The simulations in this study are under the following assumptions: i) osmotic pressure is considered to be linearly proportional to the concentration difference based on the modified van't Hoff law [36]. In the salinity range of 0-70 g/kg, the modified linear osmotic pressure approximation is validated and the maximum deviation is 6.8% [36, 37]; ii) constant hydraulic pressure difference in the membrane channel due to the negligible pressure loss; iii) significant membrane fouling and deformation do not occur; iv) For simplicity, a constant density of the water is used for both draw and feed solutions [38].

Table 3 Parameters used in the simulations of start-up of the PRO using MPPT controllers.

Parameter	Value
Concentration of the draw solution	35 g/kg
Concentration of the feed solution	0.1 g/kg
Dimensionless flow rate	0.5
Temperature	298 K
Membrane water permeability coefficient	1.06×10^{-7} m·bar^{-1}·s^{-1} [39]
Membrane salt permeability coefficient	2.62×10^{-8} m·s^{-1} [39]
Membrane structural parameter	4.62×10^{-3} m [39]
Mass transfer coefficient	4.27×10^{-4} m s^{-1} [39]

Diffusion coefficient	3.5×10^{-9} m^2 s^{-1} [39]
Density of the solutions	1,000 kg m^{-3}
Modified van't Hoff coefficient	0.7307 bar kg g^{-1} [36]
Specific membrane area	0.1 m^2 per 1 L/h feed solution
Efficiency of the HP, ERD and HT	70%, 95% and 90%

The MPPT with the four algorithms are studied in the start-up of a PRO plant. The parameters used in P&O, IMR and MFC are listed in Table 4. For the FLC based MPPT, the parameters of the membership functions of both the inputs and output are optimized by GA. The optimized membership functions are shown in Fig. 7. FLC is implemented using MATLAB fuzzy logic toolbox. The results of the power outputs using the four MPPT controllers are shown in Fig. 8. For all the MPPT controllers, the initial pressure applied on the draw solution is 1 bar and the step-pressure (including both perturbation pressure and incremental pressure) are set to be 1 bar at the first sample instant.

Table 4 Parameters of P&O, IMR and MFC.

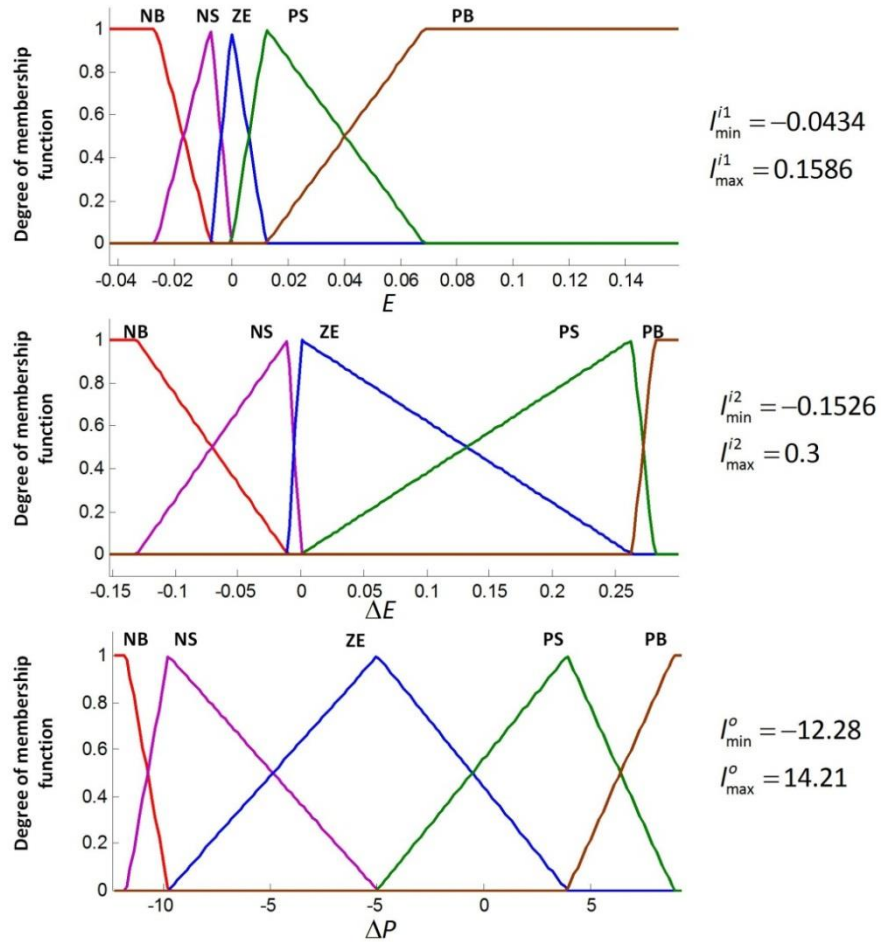| P&O		IMR		MFC	
Perturbation pressure	1 bar	Incremental pressure	1 bar	k_p	140 bar$^2 \cdot$m^2/W
		ε_{IMR}	1×10^{-3} bar or m^3/s or m^3 s^{-1} bar^{-1}	k_i	20 bar$^2 \cdot$m^2/W

Figure 7 Optimized membership functions of the three variables.

According to the results shown in Fig. 8, obviously the performance of the MPPT is significantly improved using MFC and FLC compared to that using P&O and IMR. These two controllers, FLC and MFC, are faster to reach the MPP during the start-up, and present also a much smoother signal with less fluctuation in the quasi-steady state compared to P&O. Furthermore, although IMR has better performance than P&O, using the parameter ε_{IMR} to control the oscillation may cause the slight decline of the tracked MPP as shown in Fig. 8. Also, the trade-off between the oscillation and convergence of these two MPPT controllers are determined by the fixed step-pressure which is perturbation pressure in P&O and the incremental pressure in IMR. Actually, this trade-off relationship is improved in both MFC and FLC algorithms by developing strategy of adaptive step-pressure. The adaptive strategy allows the MPPT controller employ a large step-pressure at the beginning of the start-up to achieve the fast convergence and a small step-pressure when the signal is approaching the MPP. As shown in Fig. 8, the first step-pressure in all the four algorithms is the predefined initial step-pressure (1 bar). Then, based on the measurements after the first test using the predefined fixed step-pressure, FLC and MFC adaptively increase their step-pressure which results in the significant increase on the APD of the PRO on the next sample instant. Consequently, the APD is approaching the MPP in very few steps and then the two controllers instantly reduce the step-pressure to maintain a smooth power output.
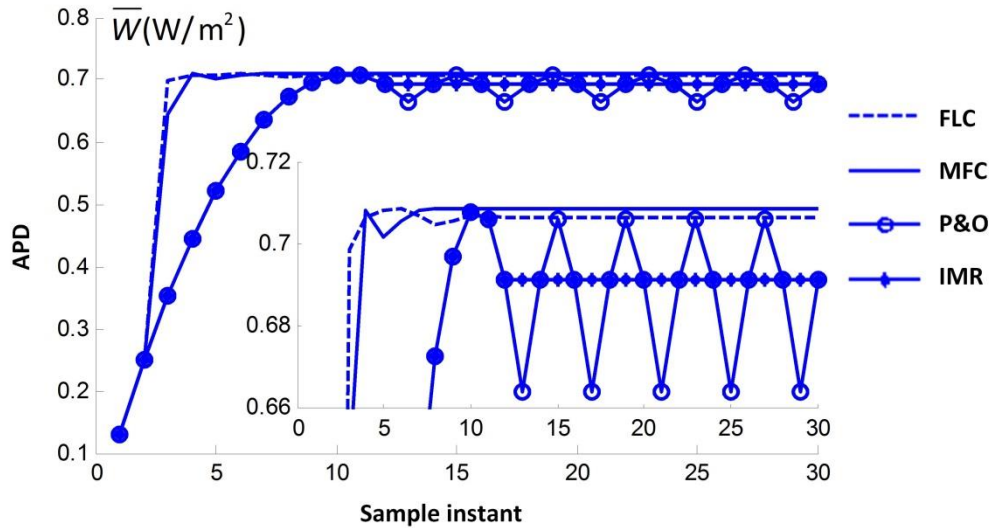
Figure 8 Power output with MPPT using P&O, IMR, MFC and FLC.

4.3. Case study of MPPT: operational fluctuations of a PRO salinity power generator

Furthermore, another case study of the MPPT controllers is presented at the operations subject to the fluctuations of the PRO plant. In fact, the PRO operation might be affected by many factors, such as temperature and applied pressure. Anastasio et al. reported that the permeability coefficients of water and solute increase from 0.589 L/(m²·bar·h) and 0.319 L/(m²·h) to 1.12 L/(m²·bar·h) and 0.580 L/(m²·h) respectively, when the temperature of the draw solution increases from 20 ^{0}C to 40 ^{0}C [40]. It also has been reported that the high pressure induced the varied membrane properties [41]. Accordingly, the MPP of PRO is also varied with respect to the changes of the operating conditions. At present, there is no explicit model or theory to address and predict the temperature effect or pressure effect on the performance of PRO plant, which makes it difficult to study the transitions between the possible MPPs considering the varying operating conditions. Because the mechanism of the temperature or pressure effect on the hydrodynamics and membrane parameters and the improvement of the membrane performance are beyond the scope of this study, all the MPPT controllers are studied and tested using the discrete parameters of the solution characteristics, hydrodynamics and membrane properties. In contrast to the operation modelling with constant parameters, the simulation uses different parameters corresponding to different steady state operation conditions with specific temperatures which are changed discretely each MPPT sample time. These tests of the MPPT controllers using the discrete parameters are also capable to verify other fluctuated operations, for instance, membrane deformation due to applied pressure changes. The parameters are from Ref [39] and shown in Table 5 in which ICP factor represents the ICP effect in the support layer. It can be used to estimate the varied structure parameter of the membrane using diffusion coefficient, $S = ICP \cdot D$. It should be noted that the parameters listed in Table 5 are usually case-dependent, which are determined by many factors, such as geometry of the membrane module, membrane properties, concentration, velocity, temperature and etc.

Table 5 Varied parameters of solution characteristics and hydrodynamics and membrane properties [39]. The draw solution studied is 35 g/kg (0.6 M approximately) NaCl solution.

Temperature (^{0}C)	A ($m \cdot s^{-1} \cdot bar^{-1}$)	B ($m \cdot s^{-1}$)	D ($m^2 \cdot s^{-1}$)	k_m ($m \cdot s^{-1}$)	ICP factor, S/D ($m^{-1} \cdot s^1$)
20	1.06×10^{-7}	2.62×10^{-8}	3.50×10^{-9}	4.27×10^{-4}	1.32×10^6
30	1.43×10^{-7}	4.25×10^{-8}	4.54×10^{-9}	9.74×10^{-4}	1.00×10^6
40	1.74×10^{-7}	5.87×10^{-8}	5.74×10^{-9}	10.88×10^{-4}	0.82×10^6
50	1.98×10^{-7}	8.00×10^{-8}	7.09×10^{-9}	11.98×10^{-4}	0.71×10^6

Based on the parameters as listed in Table 5, a series of tests are carried out to compare the four MPPT algorithms. The simulations are performed using a changing temperature profile as shown in Fig. 9. Generally, the operating temperature changes gradually in practice. For testing the controllers, simulations are carried out considering the operational temperature changes instantly, which is more difficult for MPPT to track the suddenly changed MPP. Specifically, we consider a 175 sample instants time window in which the temperature is varied. At the end of every 25 sample instants, the temperature increases or decreases by $10^{\circ}C$. The parameters and settings are same to those of the tuned MPPT controllers in the case study of the start-up. According to the simulations, the tuned MFC (tuned parameters listed in Table 3) in the case study of start-up does not have very good performance in the studied cases of state transition using parameters as shown in Table 5. A too large step pressure resulted from MFC at the 26th sample instant leads to significant decrease of process performance from $20^{\circ}C$ to $30^{\circ}C$ at the 26th. A limitation of the step pressure can be added in the MFC to avoid a too much step pressure caused by the suddenly changed operation. A simple scheme can be used to limit the step pressure, which is $\Delta P(n) = \Delta P_0$ if $\Delta P(n)$ calculated by equation (4) is larger than the limiting step pressure ΔP_{max}. DP_0 is the actuated step pressure and it can be controlled to change the performance of the MPPT but $DP_0 \leq DP_{max}$ should be considered. The results of MPPT using the modified MFC are shown in Fig. 9 and high performance can be found using the modified MFC with the selected ΔP_0 and ΔP_{max} to be 1 and 5 bar, respectively. Moreover, as shown in Fig. 9, P&O, IMR and FLC successfully tracks the varied MPP due to the changing operational temperature. The results clearly indicate the better performance of FLC than P&O and IMR. On one hand, MPPT using FLC has fast convergence at the start-up of the PRO that it reaches the MPP at the first five sample instants. On the other hand, using FLC high power outputs are tracked and low oscillation is maintained in all seven operations with different temperatures.
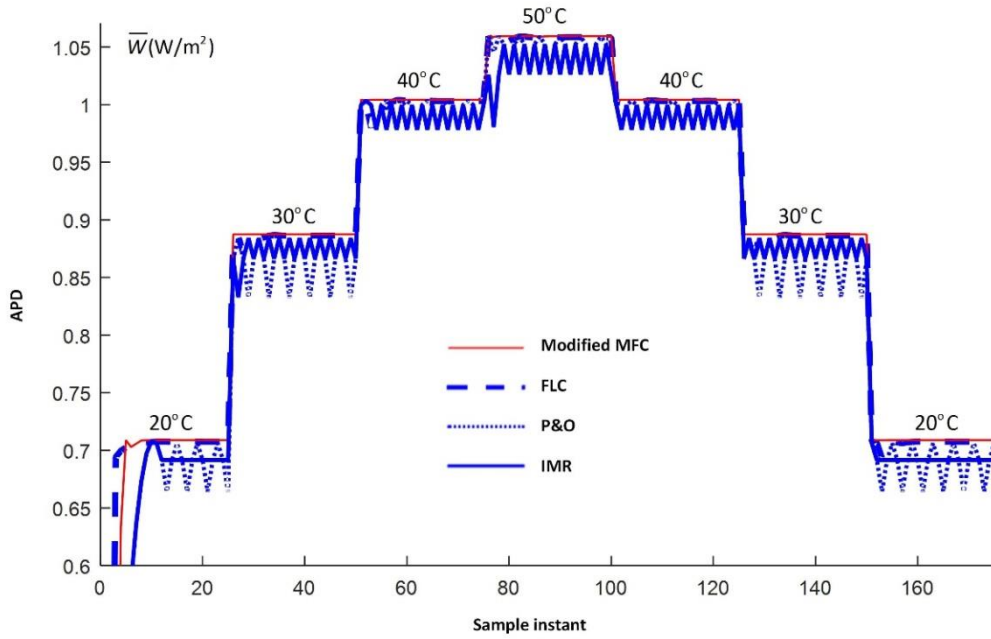
Figure 9 Power output of the PRO power plant using MPPT controllers of different algorithms subject to fluctuating operational temperatures.

Moreover, another test of these four algorithms is carried out in the case study of the PRO power plant subject to fluctuating operational concentrations and flow rates, in which both the draw solution and the feed solution are considered. Specifically, we consider a 60 sample instants time window in which the concentrations of draw and feed, and the dimensionless flow rates are changed as shown in Fig. 10 (a), 10(b) and 10(c), respectively. The dimensionless flow rate is the ratio of the flow rate of the feed to the sum of the both flow rates, which is $q_F^0 / (q_D^0 + q_F^0)$. As shown in Fig. (10), both the concentrations and the flow rates jumped suddenly to another value at particular time instants and make the operation fluctuated in the selected operation window. Tests of these four algorithms are carried out considering all the varied concentrations and dimensionless flow rates. It is important to point out that the selected fluctuated operation window is a case study and the four algorithms can be readily extended to deal with other complex fluctuation profiles. In the simulations, the membrane properties listed in Table 3 are used.
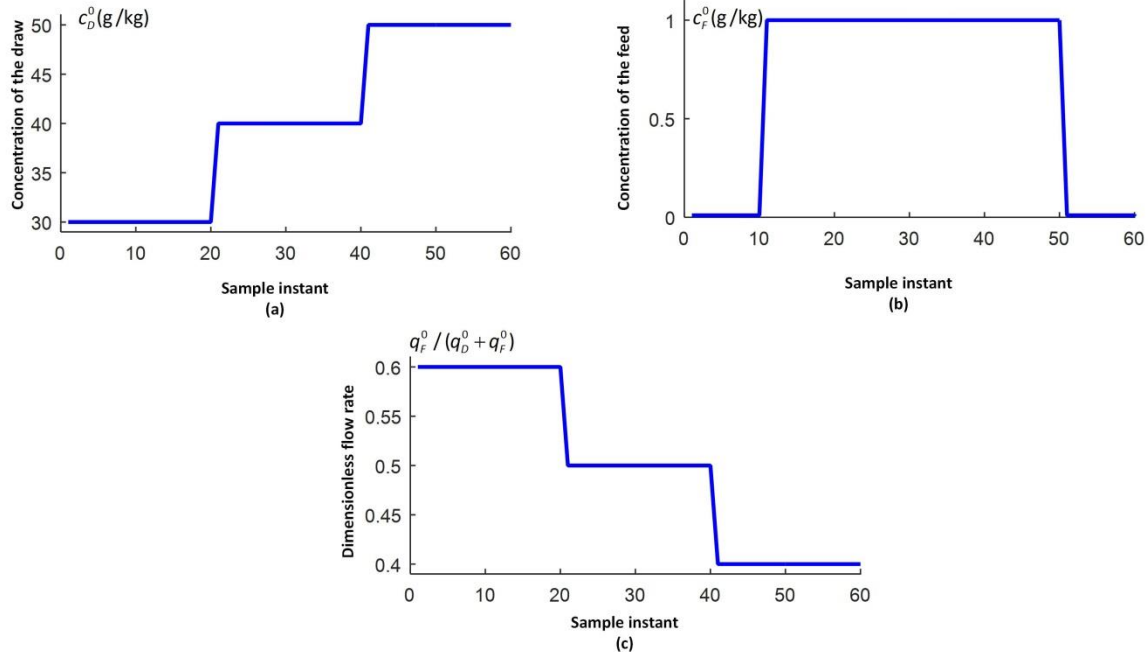
Figure 10 Variations of salinities including concentrations of the draw shown in (a) and the feed shown in (b), and the dimensionless flow rate shown in (c).

According to the fluctuating operations including both the draw and feed concentrations and dimensionless flow rate as shown in Fig. 10, the four MPPT algorithms are tested and the results are plotted in Fig. 11. Similarly to the results of MPPT dealing with fluctuated temperature, the four algorithms are capable to detect the changed operations and track the new MPPs. But it is clearly that the MPPT using FLC and modified MFC has better performance than that using P&O and IMR when the operational concentrations and flow rates of the salinities are varied. As shown in Fig. 11, both fast response to the fluctuations and smoothly tracked MPPs are found using algorithms of FLC and modified MFC.
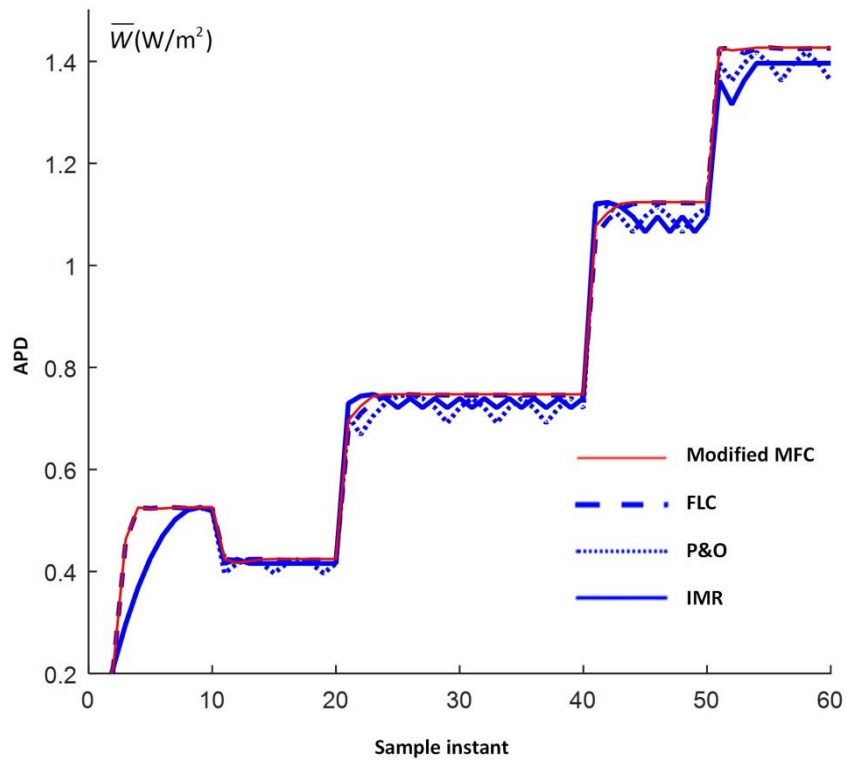
Figure 11 Power output of the PRO power plant using MPPT controllers of different algorithms subject to fluctuating operational concentrations and flow rates.

4.4.   Comparisons and discussions of MPPT controllers

A general comparison between the four MPPT algorithms considered and investigated in this study is listed in Table 6. Although the trade-off relation between the convergence and oscillation restricts the performance of the MPPT using constant step-pressure, namely P&O and IMR, both methods have advantages of low cost, independence of the PRO plant, easy implementation, stable and robust performance. In addition, MFC shows fast convergence of the MPPT at the start-up. It successfully tracks the changed MPPs under condition of the maximum step pressure restriction. Implementation of MFC controllers is relatively cheap but it needs consistent tuning for high performance. FLC algorithm has potential to balance the trade-off relation between the convergence and oscillation, and to deal with the operational fluctuations. The obtained optimized FLC demonstrates the high performance and the robustness. It has not only improved the response time in the start-up and transitional state but also reduced considerably the oscillation in the steady-state. However, the adaptive strategy behind the FLC is achieved by a series of steps and settings. The performance is determined by the experiences and knowledge of the users and designers. Compared to P&O and IMR, a better FLC-MPPT is not easy to design, parameter tuning and implement.

Table 6 Major characteristics of the four MPPT controllers.

MPPT algorithm	P&O	IMR	MFC	FLC
PRO dependent?	No	No	No	No
Analog or Digital?	Both	Digital	Digital	Digital
Periodic tuning?	No	Varies	Yes	Yes
Convergence speed	Varies	Varies	Fast	Fast
Oscillation?	Yes	No	No	No
Implementation complexity	Low	Medium	Medium	High
Vulnerable to variable operations	Low	Low	Medium	Medium

5. Conclusion

In this study, two new MPPT controllers used in the PRO power plant are proposed and evaluated, including MFC and FLC. To optimize the performance of the MPPT using FLC algorithm, GA optimization is used to find the optimum parameters for the membership functions of both the input and output variables in FLC. Then, the four MPPT controllers are compared in selected case studies. One is the start-up of the PRO and the other is the fluctuating operated PRO due to the varied temperature and salinities. Finally, based on the comparisons, the major characteristics of these four methods are presented. Therefore, according to the results, some conclusions can be drawn: 1) using MPPT at the start-up of the PRO, compared to P&O and IMR algorithms, both MFC and FLC are capable to adaptively change the step-pressure to balance the trade-off relationship between the rise-time and the steady-state oscillation; 2) optimized FLC and modified MFC algorithm are capable to deal with the operational fluctuations. MPPTs using FLC and modified MFC have the better performance than the MPPTs using P&O and IMR algorithms, meaning faster convergence and lower oscillation during all the tested start-up and steady-state transitions; 3) the comparable table can be served as a useful guide in choosing the right MPPT algorithm for a specific PRO application.

Nomenclature

A	Membrane water permeability $[\text{L} \cdot \text{m}^{-2} \cdot \text{s}^{-1} \cdot \text{bar}^{-1}]$
A_m	Membrane area $[\text{m}^2]$
B	Membrane solute permeability $[\text{L} \cdot \text{m}^{-2} \cdot \text{h}^{-1}]$
c	Concentration of solution $[\text{kg} \cdot \text{kg}^{-1}]$
C_k	Generic parameters used for designing membership functions
C_{OS}	Modified van't Hoff law coefficient $[\text{bar} \cdot \text{kg} \cdot \text{g}^{-1}]$
D	Diffusion coefficient $[\text{m}^2 \cdot \text{s}^{-1}]$
k_m	Mass transfer coefficient $[\text{m} \cdot \text{s}^{-1}]$
J_W	Water permeation flow rate $[\text{L} \cdot \text{m}^{-2} \cdot \text{h}^{-1}]$
J_S	Reverse solute permeation flow rate $[\text{L} \cdot \text{m}^{-2} \cdot \text{h}^{-1}]$
l_{min}, l_{max}	Generic parameters presenting the minimum and the maximum of a membership function
P	Pressure $[\text{bar}]$

q	Mass flow rate of solution [$\text{kg} \cdot \text{h}^{-1}$]
S	Membrane structure parameter [m]
V	Volumetric flow rate of solution [$\text{m}^3 \cdot \text{h}^{-1}$]
$\overline{W}$	Average power density [$\text{W} \cdot \text{m}^{-2}$]
x	Generic parameters used for designing membership functions
π	Osmotic pressure [bar]
ϕ	Dimensionless flow rate
η	Efficiency
ρ	Density of solution [$\text{kg} \cdot \text{m}^{-3}$]

Abbreviations

APD	Average power density
BP	Boost pump
ECP	External concentration polarization
FLC	Fuzzy logic control
HP	High-pressure pump
HT	Hydro-turbine
ICP	Internal concentration polarization
IMR	Incremental mass resistance
INC	Incremental conductance
MFC	Mass feedback control
MPP	Maximum power point
MPPT	Maximum power point tracking
NB	Negative big
NS	Negative small
PB	Positive big
P&O	Perturb & observe
PRO	Pressure retarded osmosis
PS	Positive small
PV	Photovoltaic
RO	Reverse osmosis
RSP	Reverse solute permeation
TFC	Thin-film composite
ZE	Zero

Appendix: Mathematical model of a scale-up PRO salinity power generator

In a PRO plant, the membrane power density is the product of the trans-membrane hydraulic pressure and the water permeation flux across the membrane [1]. With the scale increases, the overall performance is evaluated by integrating the water flux and power density over the entire membrane used. The modelling framework of the scale-up PRO can be found in our previous work [35]. For a clear understanding, key equations describing a PRO process are listed in Table A.1. At a particular position along the membrane channel, the water flux (equation A.1) and reverse solute flux (equation A.2) are determined by the local concentration difference between the membrane surfaces and the membrane permeability-selectivity. Based on equations (A.4) and (A.5), flow rates of the accumulative water permeation and reverse solution permeation can be obtained by

integrating the water flux and reverse salt flux. Then, update of salinities' concentration and flow rate at each position in the flow channel can be done by equations (A.6), (A.7), (A.8) and (A.9). In order to evaluate the overall efficiency of the osmotic power extraction, average power density (APD) of a scale-up PRO is expressed by equation (A.11).

Table A.1 Mathematical model of a scale-up PRO plant.

Physical quantity	Equation	NO#
Water Flux	$J_W = A(C_{os}(\dfrac{c_D \exp(-J_W / k_m) - c_F \exp(J_W S / D)}{1 + \dfrac{B}{J_W}(\exp(J_W S / D) - \exp(-J_W / k_m))}) - \Delta P_{PRO})$	(A.1)
Reverse salt flux	$J_s = B(\dfrac{c_D \exp(-J_W / k_m) - c_F \exp(J_W S / D)}{1 + \dfrac{B}{J_W}(\exp(J_W S / D) - \exp(-J_W / k_m))})$	(A.2)
Power Density	$W = J_W \cdot \Delta P_{PRO}$	(A.3)
Water Permeation	$d(\Delta V_P) = J_w d(A_m); \Delta q_P = \rho_P \Delta V_P$	(A.4)
Reverse salt permeation	$d(\Delta V_S) = J_S d(A_m); \Delta m_S = \rho_S \Delta V_S$	(A.5)
Concentration of the draw	$c_D = \dfrac{c_D^0 q_D^0 - \Delta m_S}{q_D^0 + \Delta q_P}$	(A.6)
Flow rate of the draw	$q_D = q_D^0 + \Delta q_P$	(A.7)
Concentration of the feed	$c_F = \dfrac{c_F^0 q_F^0 + \Delta m_S}{q_F^0 - \Delta q_P}$	(A.8)
Flow rate of the feed	$q_F = q_F^0 - \Delta q_P$	(A.9)
Average power density (APD)	$\overline{W} = \dfrac{\Delta P_{PRO} \Delta V_P}{V_F^0 A_m}$	(A.10)

Reference:

[1] K. Gerstandt, K.V. Peinemann, S.E. Skilhagen, T. Thorsen, T. Holt, Membrane processes in energy supply for an osmotic power plant, Desalination, 224 (2008) 64-70.
[2] Y. Li, R. Wang, S. Qi, C. Tang, Structural stability and mass transfer properties of pressure retarded osmosis (PRO) membrane under high operating pressures, Journal of Membrane Science, 488 (2015) 143-153.
[3] G. Han, S. Zhang, X. Li, T.-S. Chung, Progress in pressure retarded osmosis (PRO) membranes for osmotic power generation, Progress in Polymer Science.

[4] Y. Cui, X.-Y. Liu, T.-S. Chung, Enhanced osmotic energy generation from salinity gradients by modifying thin film composite membranes, Chemical Engineering Journal, 242 (2014) 195-203.

[5] W. He, Y. Wang, M.H. Shaheed, Energy and thermodynamic analysis of power generation using a natural salinity gradient based pressure retarded osmosis process, Desalination, 350 (2014) 86-94.

[6] E. Sivertsen, T. Holt, W.R. Thelin, G. Brekke, Iso-watt diagrams for evaluation of membrane performance in pressure retarded osmosis, Journal of Membrane Science, 489 (2015) 299-307.

[7] W. He, Y. Wang, I.M. Mujtaba, M.H. Shaheed, An evaluation of membrane properties and process characteristics of a scaled-up pressure retarded osmosis (PRO) process, Desalination, 378 (2016) 1-13.

[8] W. He, Y. Wang, A. Sharif, M.H. Shaheed, Thermodynamic analysis of a stand-alone reverse osmosis desalination system powered by pressure retarded osmosis, Desalination, 352 (2014) 27-37.

[9] J.L. Prante, J.A. Ruskowitz, A.E. Childress, A. Achilli, RO-PRO desalination: An integrated low-energy approach to seawater desalination, Applied Energy, 120 (2014) 104-114.

[10] A. Achilli, J.L. Prante, N.T. Hancock, E.B. Maxwell, A.E. Childress, Experimental Results from RO-PRO: A Next Generation System for Low-Energy Desalination, Environmental Science & Technology, 48 (2014) 6437-6443.

[11] A. Altaee, A. Sharif, G. Zaragoza, Limitations of osmotic gradient resource and hydraulic pressure on the efficiency of dual stage PRO process, Renewable Energy, 83 (2015) 1234-1244.

[12] A. Altaee, A. Sharif, G. Zaragoza, N. Hilal, Dual stage PRO process for power generation from different feed resources, Desalination, 352 (2014) 118-127.

[13] A. Altaee, N. Hilal, Design optimization of high performance dual stage pressure retarded osmosis, Desalination, 355 (2015) 217-224.

[14] A. Altaee, N. Hilal, Dual stage PRO power generation from brackish water brine and wastewater effluent feeds, Desalination.

[15] A. Altaee, N. Hilal, Dual-stage forward osmosis/pressure retarded osmosis process for hypersaline solutions and fracking wastewater treatment, Desalination, 350 (2014) 79-85.

[16] A. Altaee, A. Sharif, G. Zaragoza, A.F. Ismail, Evaluation of FO-RO and PRO-RO designs for power generation and seawater desalination using impaired water feeds, Desalination, 368 (2015) 27-35.

[17] G. Han, J. Zuo, C. Wan, T.-S. Chung, Hybrid pressure retarded osmosis-membrane distillation (PRO-MD) process for osmotic power and clean water generation, Environmental Science: Water Research & Technology, 1 (2015) 507-515.

[18] J.-G. Lee, Y.-D. Kim, S.-M. Shim, B.-G. Im, W.-S. Kim, Numerical study of a hybrid multi-stage vacuum membrane distillation and pressure-retarded osmosis system, Desalination, 363 (2015) 82-91.

[19] W. He, Y. Wang, M.H. Shaheed, Stand-alone seawater RO (reverse osmosis) desalination powered by PV (photovoltaic) and PRO (pressure retarded osmosis), Energy, 86 (2015) 423-435.

[20] K. Yeong-Chan, L. Tsorng-Juu, C. Jiann-Fuh, Novel maximum-power-point-tracking controller for photovoltaic energy conversion system, Industrial Electronics, IEEE Transactions on, 48 (2001) 594-601.

[21] S. Jain, V. Agarwal, A new algorithm for rapid tracking of approximate maximum power point in photovoltaic systems, Power Electronics Letters, IEEE, 2 (2004) 16-19.

[22] N. Femia, G. Petrone, G. Spagnuolo, M. Vitelli, Optimization of perturb and observe maximum power point tracking method, Power Electronics, IEEE Transactions on, 20 (2005) 963-973.

[23] A. Pandey, N. Dasgupta, A.K. Mukerjee, Design Issues in Implementing MPPT for Improved Tracking and Dynamic Performance, in: IEEE Industrial Electronics, IECON 2006 - 32nd Annual Conference on, 2006, pp. 4387-4391.

[24] G. Kumar, M.B. Trivedi, A.K. Panchal, Innovative and precise MPP estimation using P–V curve geometry for photovoltaics, Applied Energy, 138 (2015) 640-647.

[25] J. Ahmed, Z. Salam, A Maximum Power Point Tracking (MPPT) for PV system using Cuckoo Search with partial shading capability, Applied Energy, 119 (2014) 118-130.

[26] S.A. Rizzo, G. Scelba, ANN based MPPT method for rapidly variable shading conditions, Applied Energy, 145 (2015) 124-132.

[27] N. Bizon, On tracking robustness in adaptive extremum seeking control of the fuel cell power plants, Applied Energy, 87 (2010) 3115-3130.

[28] N. Bizon, Energy harvesting from the FC stack that operates using the MPP tracking based on modified extremum seeking control, Applied Energy, 104 (2013) 326-336.

[29] W. He, Y. Wang, M.H. Shaheed, Maximum power point tracking (MPPT) of a scale-up pressure retarded osmosis (PRO) osmotic power plant, Applied Energy, 158 (2015) 584-596.

[30] A. Messai, A. Mellit, A. Guessoum, S.A. Kalogirou, Maximum power point tracking using a GA optimized fuzzy logic controller and its FPGA implementation, Solar Energy, 85 (2011) 265-277.

[31] C. Larbes, S.M. Aït Cheikh, T. Obeidi, A. Zerguerras, Genetic algorithms optimized fuzzy logic control for the maximum power point tracking in photovoltaic system, Renewable Energy, 34 (2009) 2093-2100.

[32] A.R. Bartman, A. Zhu, P.D. Christofides, Y. Cohen, Minimizing energy consumption in reverse osmosis membrane desalination using optimization-based control, Journal of Process Control, 20 (2010) 1261-1269.

[33] A.R. Bartman, P.D. Christofides, Y. Cohen, Nonlinear model-based control of an experimental reverse-osmosis water desalination system, Industrial & Engineering Chemistry Research, 48 (2009) 6126-6136.

[34] K.M. Sassi, I.M. Mujtaba, Optimal operation of RO system with daily variation of freshwater demand and seawater temperature, Computers & Chemical Engineering, 59 (2013) 101-110.

[35] W. He, Y. Wang, M.H. Shaheed, Modelling of osmotic energy from natural salt gradients due to pressure retarded osmosis: Effects of detrimental factors and flow schemes, Journal of Membrane Science, 471 (2014) 247-257.

[36] M.H. Sharqawy, L.D. Banchik, J.H. Lienhard V, Effectiveness–mass transfer units (ε–MTU) model of an ideal pressure retarded osmosis membrane mass exchanger, Journal of Membrane Science, 445 (2013) 211-219.

[37] L.D. Banchik, M.H. Sharqawy, J.H. Lienhard V, Effectiveness-mass transfer units (ε-MTU) model of a reverse osmosis membrane mass exchanger, Journal of Membrane Science, 458 (2014) 189-198.

[38] G.A. Fimbres-Weihs, D.E. Wiley, Numerical study of two-dimensional multi-layer spacer designs for minimum drag and maximum mass transfer, Journal of Membrane Science, 325 (2008) 809-822.

[39] K. Touati, F. Tadeo, C. Hänel, T. Schiestel, Effect of the operating temperature on hydrodynamics and membrane parameters in pressure retarded osmosis, Desalination and Water Treatment, (2015) 1-13.

[40] D.D. Anastasio, J.T. Arena, E.A. Cole, J.R. McCutcheon, Impact of temperature on power density in closed-loop pressure retarded osmosis for grid storage, Journal of Membrane Science, 479 (2015) 240-245.

[41] Q. She, Y.K.W. Wong, S. Zhao, C.Y. Tang, Organic fouling in pressure retarded osmosis: Experiments, mechanisms and implications, Journal of Membrane Science, 428 (2013) 181-189.